Università degli Studi di Roma Tor Vergata

Direct numerical simulation of the pulsatile flow through an aortic bileaflet mechanical heart valve

Pierluigi Morra

Supervisor: Roberto Verzicco

Why?

Despite their widespread clinical use, mechanical heart valve implants still carry significant risks such as:

- Haemolysis
- Platelet activation
- Thrombosis

Those problems can be associated both to the blood flow through the mechanical valve and to the geometry of the valve itself

- The mechanical heart valve itself introduces pressure drops and areas for formation of clots
- The turbulence of the blood flow can be associated to platelet activation and haemolysis

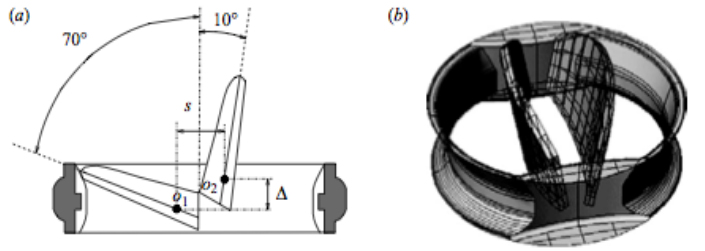

FIGURE 1. (*a*) Range of rotation of the leaflets. (*b*) Geometrical model of the reproduced valve.

Mechanical Heart Valve (MHV) Characteristics

- The valve model considered resembles the 27 mm Bicarbon model used in the experiments
- The two leaflets are placed symmetrically and have a curved profile
- Each of the three orifice areas introduces equal resistance to blood flow
- The leaflets can virtually rotate without sliding. This introduces a small axial displacement Δ
- The friction to rotation is minimized and there is an uninterrupted washing of the exposed surfaces

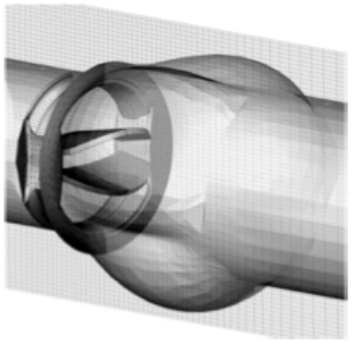

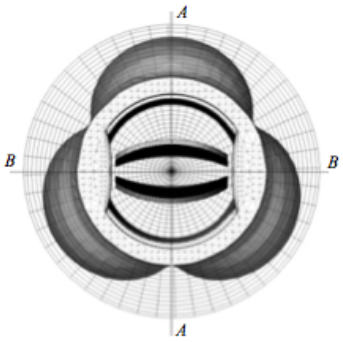

MHV–Aortic Root Coupling

The geometry of the aortic root reproduces the model used for the experimental investigations and corresponds to the physiological case

- The aortic root has the 3 Valsalva sinuses in an axisymmetric configuration
- The material does not have characteristics similar to the heart tissues

The valve is mounted in:

- an intra-annular configuration: the valve housing does not extend into the three sinuses
- an asymmetric orientation with respect to the sinuses

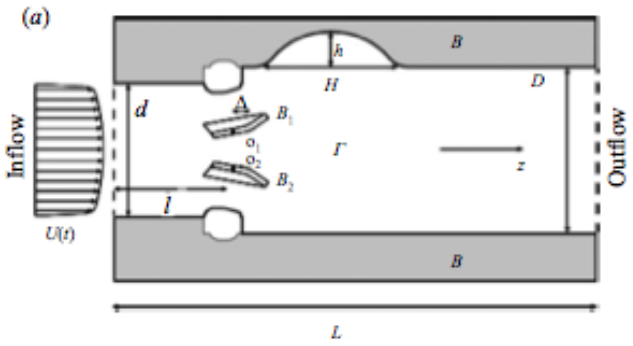

Figure (a): a bi-dimensional sketch of the MHV-Aortic Root configuration with the dimensions of the structure:

$D = 1.26d$, $l = d$, $L = 5d$, $H = 1.14d$ and $h = 0.26d$

The inflow velocity U(t) is modulated in time to mimic the physiological flow rate produced by the heart

The equations

NOTE: The fluid model is Newtonian, since blood in large arteries behaves accordingly

The set of governing equations is:

$$(1) \quad \frac{\partial \boldsymbol{u}}{\partial t} + \nabla \cdot (\boldsymbol{u}\boldsymbol{u}) = -\nabla p + \frac{1}{Re}\nabla^2 \boldsymbol{u} + \boldsymbol{f},$$

$$\nabla \cdot \boldsymbol{u} = 0, \text{ on } \Gamma$$

$$(2) \quad I_i \frac{\mathrm{d}^2\theta_i}{\mathrm{d}t^2} = T_i, \quad M_i \frac{\mathrm{d}^2 z_i}{\mathrm{d}t^2} = F_i \quad \text{for } B_i \text{ with } i = 1, 2$$

$$(3) \quad T_i = \int_{S_i} [(\boldsymbol{\tau} \cdot \boldsymbol{n} - p\boldsymbol{n}) \times \boldsymbol{r}] \cdot \hat{\boldsymbol{x}} \, \mathrm{d}S \quad \text{and} \quad F_i = \int_{S_i} (\boldsymbol{\tau} \cdot \boldsymbol{n} - p\boldsymbol{n}) \cdot \hat{\boldsymbol{z}} \, \mathrm{d}S, \quad i = 1, 2$$

where B_i are the valve leaflets, Γ is the time-dependent fluid domain, $\boldsymbol{u}$ the velocity vector, p the pressure, τ the viscous stress tensor, $\boldsymbol{n}$ the outer normal to the surface S_i of the ith leaflet, $\boldsymbol{r}$ the vector given by the distance from the axis to the surface element $\mathrm{d}S$, $\boldsymbol{f}$ the direct forcing of the immersed boundary method.

Fluid solver

$$(1) \quad \frac{\partial \boldsymbol{u}}{\partial t} + \nabla \cdot (\boldsymbol{uu}) = -\nabla p + \frac{1}{Re}\nabla^2 \boldsymbol{u} + \boldsymbol{f}$$

Equation (1) is solved by means of an immersed boundary method where the $\boldsymbol{f}$ is an "artificial" forcing used to impose the presence of the time-dependent boundary.

$$\frac{\hat{\boldsymbol{u}} - \boldsymbol{u}^l}{\Delta t} = -\alpha_l \nabla p^l - [\gamma_l \nabla (\boldsymbol{uu})^l + \rho_l \nabla (\boldsymbol{uu})^{l-1}] + \frac{\alpha_l}{2Re}\nabla^2 (\hat{\boldsymbol{u}} + \boldsymbol{u}^l) + \boldsymbol{f}^{l+\frac{1}{2}}$$

$$\boldsymbol{u}^{l+1} = \hat{\boldsymbol{u}} - \alpha_l \Delta t \nabla \phi^{l+1} \qquad p^{l+1} = p^l + \phi^{l+1} - \frac{\alpha_l \Delta t}{2Re}\nabla^2 \phi^{l+1}$$

Where ϕ is found by computing the divergence of the previous relation:

$$\nabla^2 \phi^{l+1} = \frac{\nabla \cdot \hat{\boldsymbol{u}}}{\alpha_l \Delta t}$$

Leaflets solver

$$(2) \quad I_i \frac{\mathrm{d}^2\theta_i}{\mathrm{d}t^2} = T_i, \quad M_i \frac{\mathrm{d}^2 z_i}{\mathrm{d}t^2} = F_i \quad \text{for } B_i \text{ with } i = 1, 2$$

The equation are expanded to a system of first-order ordinary ODE in $\theta_i,\ \dot{\theta}_i,\ z_i,\ \dot{z}_i$ with generalized loads on the right hand side L_{ij}, $i = 1, 2$ and $j = 1, 4$.

- An under-relaxation of the loads is used and $L_{ij} = \gamma L_{ij}^{l} + (1 - \gamma) L_{ij}^{l-1}$ and $\gamma = 0.9$
- The value 0.9 was maintained fixed in time
- Its value has been chosen by a trial-and-error process using preliminary coarse numerical simulation
- Even though the value 0.9 might not be optimal the convergence of the algorithm is achieved with an error below the prescribed tolerance (10^{-4})

Fluid & Leaflets Solvers Coupling

The fluid solver is then coupled with the leaflets solver as follows:

a) Find ${}^{p}\theta_j,\ {}^{p}\dot{\theta}_j,\ {}^{p}z_j,\ {}^{p}\dot{z}_j$ by using (2), with $F_j,\ T_j$ computed from $\boldsymbol{u}$ and p at the previous time step

b) Find $\boldsymbol{u}$ and p using (1), with the boundary conditions provided by (a), and compute the new resulting $F_j,\ T_j$ through (3)

c) Compute ${}^{c}\theta_j,\ {}^{c}\dot{\theta}_j,\ {}^{c}z_j,\ {}^{c}\dot{z}_j$ using (2)

d) Check for convergence: If $e_j = |{}^{c}\dot{\theta}_j - {}^{p}\dot{\theta}_j| > 10^{-4}$, repeat steps ($b$) to ($d$) and check again convergence with ${}^{p}\dot{\theta}_j := {}^{c}\dot{\theta}_j$ and ${}^{c}\dot{\theta}_j$ recomputed from (2) (the same operations are also performed on $\theta_i,\ z_i$ and $\dot{z}_i$)

The computations were performed with a fixed Courant number $CFL = \Delta t \left(\frac{u_x}{\Delta x} + \frac{u_y}{\Delta y} + \frac{u_z}{\Delta z} \right)$

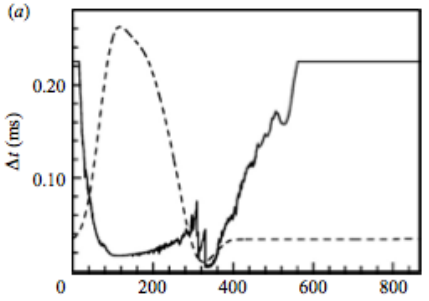

Flow parameters

- Inflow diameter $d = 27mm$
- Reynolds number $Re = Ud / \nu = 7200$ calculated with the inflow peak velocity $U = 0.81\ ms^{-1}$, a blood kinematic viscosity $\nu = 3.04 \times 10^{-6}\ m^2 s^{-1}$ and the inflow diameter d
- Leaflet density $\rho_l = 2000\ \mathrm{kgm}^{-3}$
- Blood density $\rho_b = 1060\ \mathrm{kgm}^{-3}$
- Leaflet mass $M_j = 4.086 \times 10^{-4}\ kg$ and moment of inertia $I_j = 7.947 \times 10^{-9}\ kg\ m^2$
- Integration time interval nT, with $n = 1, 2, \ldots$ and T = 866 ms (one heart cycle)

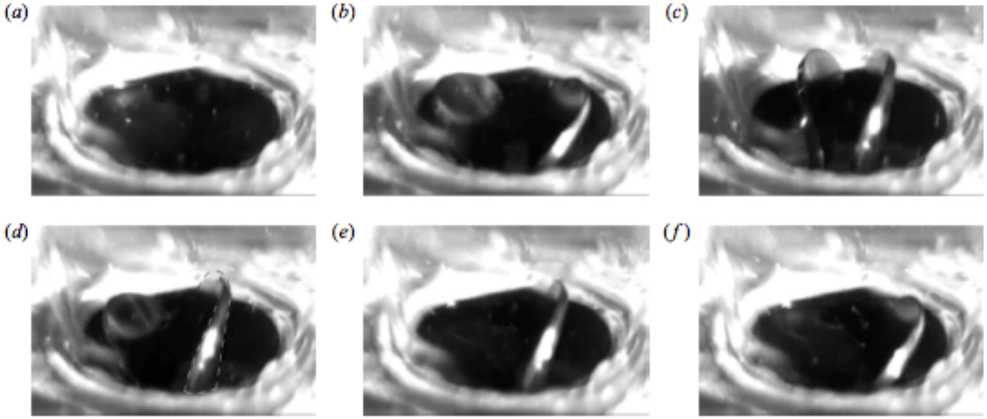

FIGURE 9. Instantaneous snapshots of the valve leaflets dynamics from an experimental visualization: (*a*) $t \simeq 0$ ms, (*b*) $t \simeq 30$ ms, (*c*) $t \simeq 60$ ms, (*d*) $t \simeq 250$ ms, (*e*) $t \simeq 310$ ms, (*f*) $t \simeq 340$ ms. Courtesy of G. P. Romano, reproduced with permission.

Leaflets Dynamics

The opening:

- Fast acceleration at the beginning
- Initial axial motion without appreciable rotation
- Deceleration due to fluid-structure interaction
- Final axial alignment at a velocity near to naught

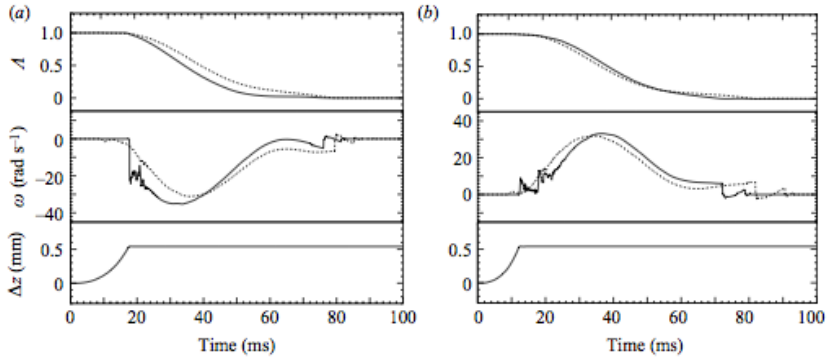

FIGURE 13. Opening phase: time variation (in ms) of the phase-averaged leaflets' angular position $\Lambda = (\alpha_{open} - \alpha)/(\alpha_{open} - \alpha_{closed})$ (top), angular velocity (middle) and axial displacement (bottom). (*a*) Leaflet 1, (*b*) leaflet 2. (———) valve with axial displacement and (·····) without axial displacement.

The closing:

- Smooth change in angular velocity
- Constant increase in angular velocity (higher values than in the opening)
- Final high speed hit against the housing
- Oscillations due to leakages and collisions neglected

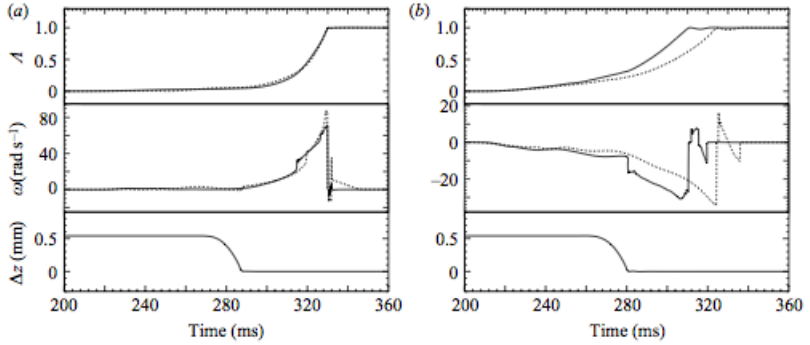

FIGURE 14. Closing phase: time variation (in ms) of the phase-averaged leaflets' angular position $\Lambda = (\alpha_{open} - \alpha)/(\alpha_{open} - \alpha_{closed})$ (top), angular velocity (middle) and axial displacement (bottom). (*a*) Leaflet 1, (*b*) leaflet 2. (———) valve with axial displacement and (·····) without axial displacement.

Peak Stresses

Turbulent stresses are only part of the solicitation on a fluid particle, the other part being the viscous stresses.

- At the red cell scale turbulent stresses are negligible compared to the viscous stresses

What really matters in red cell damaging is the amount of time red cells are subjected to stresses.

- A Lagrangian approach is needed to track the stress history of single fluid particles

Peak Stresses

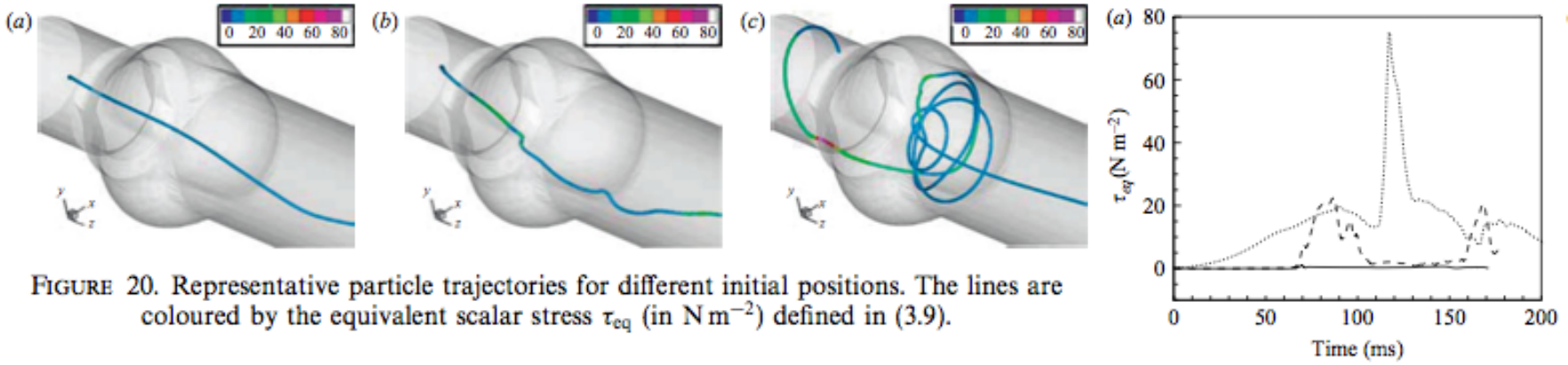

FIGURE 20. Representative particle trajectories for different initial positions. The lines are coloured by the equivalent scalar stress τ_{eq} (in N m^{-2}) defined in (3.9).

Three different fluid particle trajectories examples and their relative equivalent stress behaviours in time.

The equivalent stress was computed by means of the Von Mises criterion, which equates the work of a fluid element in a plain shear flow with the work for a full three-dimensional deformation, leading to:

$$\tau_{eq} = \frac{1}{\sqrt{3}}\sqrt{\tau_{11}^2 + \tau_{22}^2 + \tau_{33}^2 - \tau_{11}\tau_{22} - \tau_{22}\tau_{33} - \tau_{11}\tau_{33} + 3(\tau_{12}^2 + \tau_{23}^2 + \tau_{13}^2)}$$

Conclusions

- A numerical tool for studying the pulsatile flow in a MHV with a realistic geometry of the aortic root has been developed
- It has been shown to be accurate and efficient
- Though comparable in magnitude, viscous stresses have been shown to increase risk of haemolysis more so than turbulent stresses

That's all folks!

Thank you for your attention